Wind vector estimation considering difference of propeller model characteristics for fully actuated drone

Manto Kamiya, Sakahisa Nagai, and Hiroshi Fujimoto

Abstract— **Recently force control for drones is receiving interest. One of the challenges to conduct force control for drones is the separation of wind disturbance from total disturbance. This paper focuses on the method which can apply fully actuated drones whose propellers are mounted in different directions. The wind disturbance estimation is conducted based on blade element theory. Our last proposed method has not considered the difference between the propellers' characteristics which can cause the estimation error. In this paper, we propose a new estimation method to improve the estimation accuracy compared with our conventional wind vector estimation method. The proposed method considers the model of each propeller and solves the non-linear equation using an optimization method. The proposed method is compared with the conventional method and its effectiveness is confirmed by simulations and bench experiments.**

I. Introduction

Recently, business which utilizes multi-rotor Unmanned Aerial Vehicles (UAV) is rapidly developing and the market is expected to grow continuously [1]. In such situations, large-size multi-rotor UAVs for industrial fields are developing [2]. There are two advantages to use large multi-rotor UAVs. First of all, a large multi-rotor UAV is capable of lifting heavy payloads, such as large cargo or heavy equipment for inspection. In addition, according to the momentum theory, it is efficient to use large propellers with low rotational speed to generate thrust.

Conventionally, multi-rotor UAVs have been mainly used to take aerial images or to carry packages with one multi-rotor UAV and many themes have been studied such as trajectory tracking control [3]. On the other hand, the demand for applications of multi-rotor UAVs to interact with the surrounding environment will increase in the future. For example, it is considered to use multi-rotor UAVs for co-operative payload transportation [4] or contact inspection on buildings and bridges [5]. When multi-rotor UAVs conduct such missions, it is effective to implement force control [4].

A fully actuated multi-rotor UAV is a drone whose propellers are oriented in different directions. It is currently receiving interest as one of the suitable UAVs for high-precision applications including force control. Since a multi-rotor UAV with parallel propellers is an underactuated system, it is impossible to control six DOF motion independently. On the other hand, as shown in Fig. 1, mounting propellers in different directions allows the drones to control their six DOF motion separately [6], [7]. This means that a

M. Kamiya, S. Nagai, H. Fujimoto are with Graduate School of Frontier Science, The University of Tokyo, 5-1-5, Kashiwanoha, Kashiwa, Chiba, 277-8561, Japan
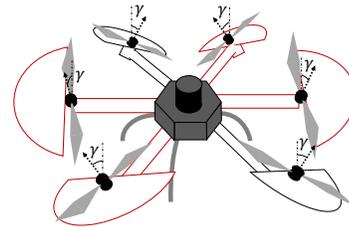
Fig. 1. Fully actuated drone.

fully actuated drone is able to achieve translational motion without tilting its body. Taking advantage of this feature, a fully actuated drone is expected to be used in situations where force control is required, such as contact inspections [8].

One of the significant difficulties of force control for outdoor multi-rotor UAVs is wind disturbance. The force caused by a wind disturbance should be separated from others to recognize non-wind force accurately and to implement force control. Hence, it is important to estimate a wind vector that flows into the multi-rotor UAV to distinguish the force caused by wind and non-wind force.

Some methods were proposed to date to estimate wind vectors with multi-rotor UAVs as follows:

1) Using external wrench estimation with an Inertial Measurement Unit (IMU) [9]
2) Using the relationship between a tilt angle and wind velocity with an IMU [10]
3) Considering dynamics of motors and propellers [11], [12]

However, as mentioned in [12], method 1 and method 2 have difficulty in separating force caused by wind and non-wind force because the external force applied to the body frame of multi-rotor UAVs is basically considered only as a wind disturbance in those methods. Method 3 which considers the dynamics of the motor and propeller has the potential to estimate wind vector and to separate force caused by wind from other force. Reference [11] is a previous work of wind vector estimation for force control of drones which considers motor and propeller dynamics. The power of motor and blade momentum theory are used for the estimation. Its method attempts to estimate three-dimensional wind velocity by combining physical models and machine learning. The method is verified by applying the algorithm which is generated from the data of a drone to the offline data set. However, the method has numerically complicated steps.
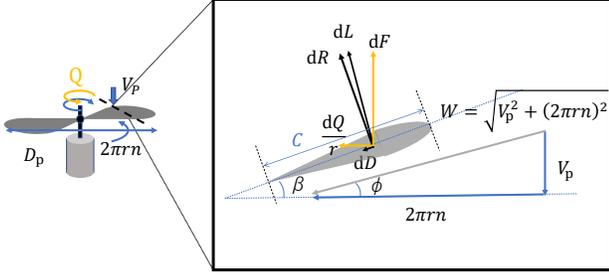
Fig. 2. Velocities and force acting on propeller blade element.

In addition, the research concluded that it is low accuracy to estimate wind velocity only with physical model. This is why machine learning is combined with the model-based method in this paper. Reference [12] is our previous method. Blade element theory, counter torque of propeller and fully actuated drone were focused on in the paper. It proposed a simple wind vector estimation method only by utilizing the tilted propellers of a fully actuated drone and physical-based model. The estimation method which uses physical-based models can be robust to unforeseen circumstances. The study showed the possibility of simple wind vector estimation with the bench test in a wind tunnel.

The wind vector estimation of method 1 and method 2 have difficulty in separating force caused by wind and non-wind force without additional equipment. Therefore this paper focuses on the method in [12]. The purpose of this paper is to propose a potentially improved method of wind vector estimation which uses simple model and recursive least-square (RLS). The proposed method takes into account the difference of characteristics among propellers while our previous method does not consider.

This paper is organized as follows: Section 2 describes the modeling of a propeller. A method of the new wind vector estimation is proposed in Section 3. Simulations are shown in Section 4. Finally, the experiments are discussed in Sections 5 and 6.

II. Modeling of Motor and Propeller

In this section, the dynamics of the motor and propeller are focused on. The dynamics of the propeller is described with blade element theory.

The equation of motion of the electric motor is described as follows:

$$T^* - Q = 2\pi J_\omega \frac{\mathrm{d}n}{\mathrm{d}t} + 2\pi B_\omega n + T_c, \qquad (1)$$

where T^* is torque reference, J_ω is inertia moment of propeller, B_ω is viscosity coefficient of propeller, and T_c is coulomb friction. Q is counter torque to motors which is applied in the opposite direction of propeller rotation by the wind. n is the rotational speed of the propeller. Thrust F and

counter torque Q of the propeller are described as follows:

$$F = C_F(J)\rho n^2 D_\mathrm{p}^4, \qquad (2)$$

$$Q = C_Q(J)\rho n^2 D_\mathrm{p}^5. \qquad (3)$$

ρ is air density and D_p is the propeller diameter. C_F is coefficient of thrust and C_Q is coefficient of torque. The blade angle β is fixed in this paper. C_F and C_Q are often described as a function of advance ratio J which is defined as

$$J = \frac{V_\mathrm{p}}{nD_\mathrm{p}}. \qquad (4)$$

The relationship between thrust F, counter torque Q and wind velocity V_p which flows into the propeller is explained by blade element theory. Fig. 2 shows force and wind velocities acting on the propeller blade element. The blade element is the part which is r away from the center and has a thickness of $\mathrm{d}r$. According to Fig. 2, $\mathrm{d}L$ and $\mathrm{d}D$ are lift and drag acting on the blade element. $\mathrm{d}L$ and $\mathrm{d}D$ are calculated by

$$\mathrm{d}L = \frac{1}{2}\rho C_L c \mathrm{d}r W^2, \qquad (5)$$

$$\mathrm{d}D = \frac{1}{2}\rho C_D c \mathrm{d}r W^2, \qquad (6)$$

where

$$W = \sqrt{V_\mathrm{p}^2 + (2\pi rn)^2}. \qquad (7)$$

c is the chord length, C_L is the lift coefficient, and C_D is the drag coefficient. W is the resultant velocity of airflow velocity and rotational speed. Let B be the number of the blades, the total thrust F and the total counter torque Q of the propeller is described as follows:

$$F = B \int \mathrm{d}F = B \int (\mathrm{d}L \cos\phi - \mathrm{d}D \sin\phi), \qquad (8)$$

$$Q = B \int \mathrm{d}Q = B \int r(\mathrm{d}L \sin\phi + \mathrm{d}D \cos\phi). \qquad (9)$$

According to Fig. 2, ϕ is determined by the ratio of V_p to the air velocity flowing laterally into the blades. Thus ϕ is obtained as

$$\tan\phi = \frac{V_\mathrm{p}}{2\pi nr} = \frac{J}{\pi \frac{2r}{D_\mathrm{p}}}. \qquad (10)$$

According to (5)-(9), the total thrust F and total counter torque Q are calculated by integrating (8) and (9) with respect to r. Therefore C_F and C_Q are considered as a function of J.

III. Wind Vector Estimation for Fully Actuated Drone

In this section, the new wind vector estimation method for fully actuated drones which considers the difference of propeller characteristics is proposed. The proposed method requires a degree of freedom in the direction of propellers. Therefore, fully actuated drones are focused on. In addition, as mentioned in [12], it is difficult to estimate wind vectors with high rotational speed by using this method. Hence, large-size industrial fully actuated drones which hover with low rotational speed are the targets of the application in this
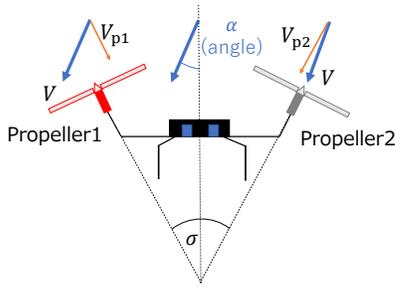
Fig. 3. Configuration of propellers of fully actuated drone.

paper. As shown in Fig. 3, the case of two propellers is considered in this paper to simplify the situation.

The wind vector estimation method in [12] will be referred as "conventional method" in this paper. Both the conventional and proposed methods estimate the velocities V_{p} of airflow through the propellers by using observer at the first step. Then, the wind vector through the body of the fully actuated drone is estimated by using the estimated V_{p} and configuration of the propellers of the drone. The conventional method uses RLS method to estimate wind vectors. The model function of the relationship between airflow angle to a propeller and V_{p} of each propeller is considered to be common among all propellers in the conventional method. On the other hand, the proposed method takes into account the difference of the model function between propellers and estimates wind vector by minimizing the L_2 norm of the error between the calculation value from the model and the estimation value. The overall estimation block diagram is shown in Fig. 4.

A. Airflow Velocity Estimation

In the first step, the observer-based V_{p} estimation method is used. Note that I is motor current. Rotational speed n and counter torque Q are considered as the state variables and the state space equation is described as follows:

$$\dot{\mathbf{x}} = \mathbf{A}\mathbf{x} + \mathbf{B}I, \qquad n = \mathbf{C}\mathbf{x}, \qquad (11)$$

where $\mathbf{A}$, $\mathbf{B}$, $\mathbf{C}$ and $\mathbf{x}$ are defined as follows:

$$\mathbf{A} = \begin{pmatrix} -\frac{B_\omega}{J_\omega} & -\frac{1}{J_\omega} \\ 0 & 0 \end{pmatrix}, \quad \mathbf{B} = \begin{pmatrix} \frac{K}{J_\omega} \\ 0 \end{pmatrix},$$

$$\mathbf{C} = \begin{pmatrix} \frac{1}{2\pi} & 0 \end{pmatrix}, \quad \mathbf{x} = \begin{pmatrix} \omega \\ Q \end{pmatrix}. \qquad (12)$$

The motor torque is accurately estimated from the motor current and thus, the effects of V_{p} are estimated from the information of the motor current and propeller model. The thrust control of propellers which uses this fact is proposed by [13]. The idea of airspeed estimation using motor torque was proposed in [14] and adapted to the observer-based estimation scheme in [15]. From (11), Q is estimated as a disturbance of the motor by using an observer [16]. C_Q usually has an inverse function of J in the operating region. Therefore, V_{p} of each two propellers is designated

by estimated Q as follows:

$$\hat{V}_{\mathrm{p1}} = n_1 D_{\mathrm{p1}} C_{Q1}^{-1}\left(\frac{\hat{Q}_1}{\rho n_1^2 D_{\mathrm{p1}}^5}\right), \qquad (13)$$

$$\hat{V}_{\mathrm{p2}} = n_2 D_{\mathrm{p2}} C_{Q2}^{-1}\left(\frac{\hat{Q}_2}{\rho n_2^2 D_{\mathrm{p2}}^5}\right). \qquad (14)$$

As shown in Fig. 3, V_{p1} is V_{p} of propeller 1 and V_{p2} is V_{p} of propeller 2.

B. Relationship Between Airflow Velocity Flowing in Propellers and Wind Vector

Wind vector is estimated by using the estimated $\hat{V}_{\mathrm{p1}}$ and $\hat{V}_{\mathrm{p2}}$. It is considered that the case where V flows in at an angle of a to the propeller. The model function of angular sensitivity of V_{p} to V will be referred to as "Angular sensitivity function" in this paper. In this study, the angular sensitivity function is experimentally obtained as follows:

$$\frac{V_{\mathrm{p}}}{V} = \cos(wa + \psi), \qquad (15)$$

where w and ψ are fitting parameters. Therefore, V_{p1} and V_{p2} in Figs. 3 and 4 are calculated by

$$\frac{V_{\mathrm{p1}}}{V} = \cos\left(w\left(\frac{\sigma}{2} + \alpha\right) + \psi\right), \qquad (16)$$

$$\frac{V_{\mathrm{p2}}}{V} = \cos\left(w\left(\frac{\sigma}{2} - \alpha\right) + \psi\right). \qquad (17)$$

Note that σ is a predefined parameter.

C. Conventional Method: Wind Vector Estimation Using RLS

In the conventional method, the angular sensitivity function (16)–(17) are defined with the same parameters w and ψ for all propellers to simplify the model and to use RLS. The average of V_{p1} and V_{p2} of each airflow angle is used to obtain w and ψ by fitting experimental data. RLS is used by transforming (16) and (17) into the following equation:

$$Y = \eta\theta, \qquad (18)$$

where Y, η and θ is defined as follows:

$$Y = \left(V_{\mathrm{p2}} - V_{\mathrm{p1}}\right)\cos\left(\frac{w\sigma}{2} + \psi\right), \qquad (19)$$

$$\eta = \left(V_{\mathrm{p1}} + V_{\mathrm{p2}}\right)\sin\left(\frac{w\sigma}{2} + \psi\right), \qquad (20)$$

$$\theta = \tan(w\alpha). \qquad (21)$$

Considering the conditions which are specific to multi-rotor UAVs such as slow airflow velocity into propellers, updating rules of RLS are divided into two cases to avoid zero dividing when η is almost zero. The same updating rules of parameters in [12] are used in this paper.

Finally, airflow angle $\hat{\alpha}[k]$ is estimated by

$$\hat{\alpha}[k] = \frac{1}{w}\arctan\hat{\theta}[k]. \qquad (22)$$

The airflow velocity V is estimated by

$$\hat{V} = \frac{1}{2}\left(\frac{\hat{V}_{p1}}{\cos\left(w\left(\frac{\sigma}{2} + \hat{\alpha}\right) + \psi\right)} + \frac{\hat{V}_{p2}}{\cos\left(w\left(\frac{\sigma}{2} - \hat{\alpha}\right) + \psi\right)}\right). \qquad (23)$$
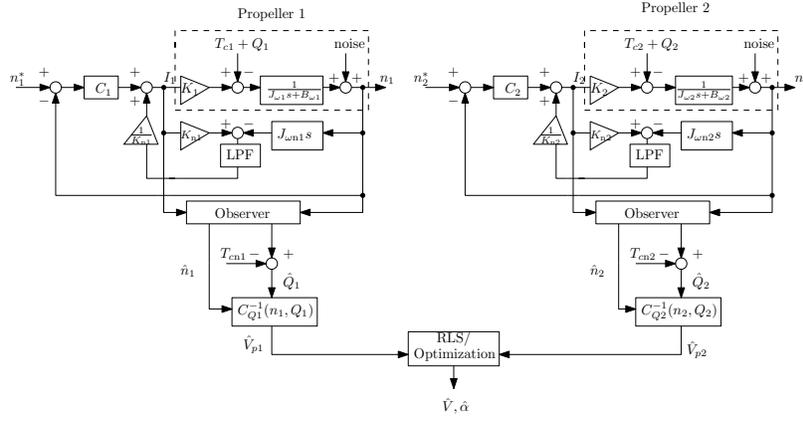
Fig. 4. Wind vector estimator.

D. Proposed Method: Wind Vector Estimation Considering Non-linear Simultaneous Equation

In reality, the angular sensitivity function can be differ among each propeller because of manufacturing variations. The proposed method considers the difference of the angular sensitivity function of each propeller. RLS is difficult to be used because w and ψ are not the same among all propellers. Thus, V and α are estimated by considering (16)–(17) as non-linear simultaneous equation. However, the following issues exist when solving non-linear simultaneous equations. First, solving non-linear simultaneous equations are computationally expensive. Second, it is susceptible to measurement noise or error of models. Therefore (16)–(17) are transformed into the optimization problem to avoid these issues in the proposed method. The optimization problem is defined as follows:

$$\min_{-\frac{\pi}{2} \le \alpha \le \frac{\pi}{2}, V \in \mathbf{R}} F(\alpha, V). \tag{24}$$

Where $F(\alpha, V)$ is defined as follows:

$$F(\alpha, V) = e_1^2 + e_2^2 + f_b, \tag{25}$$

$$e_1 = \hat{V}_{p1} - V \cos\left(w_1 \left(\frac{\sigma}{2} + \alpha\right) + \psi_1\right), \tag{26}$$

$$e_2 = \hat{V}_{p2} - V \cos\left(w_2 \left(\frac{\sigma}{2} - \alpha\right) + \psi_2\right), \tag{27}$$

$$f_b = \exp\left(10\left(\alpha - \frac{2\pi}{3}\right)\right) + \exp\left(-10\left(\alpha + \frac{2\pi}{3}\right)\right). \tag{28}$$

Note that f_b is a barrier function to limit the searching area of α. The meaning of this optimization is to search V and α minimizing the L_2 norm of the error between the calculation value from the model and the estimation value of $V_{\rm p}$. Estimated V and α are updated based on the steepest descent method. The updating rules are defined as follows:

$$p_{k+1} = p_k - d \cdot \nabla F(p_k), \tag{29}$$

$$p_k = \begin{pmatrix} \alpha_k \\ V_k \end{pmatrix}, \nabla F = \begin{pmatrix} \frac{\partial F}{\partial \alpha} \\ \frac{\partial F}{\partial V} \end{pmatrix}. \tag{30}$$

d is a parameter of optimization step size which is able to adjust estimation speed and noise.

(a) Experimental data of C_{Q1}

(b) Experimental data of C_{Q2}

(c) Experimental data of angle sensitivity

(d) $V_{\rm p}$ estimation

(e) Wind velocity estimation

(f) Airflow angle estimation
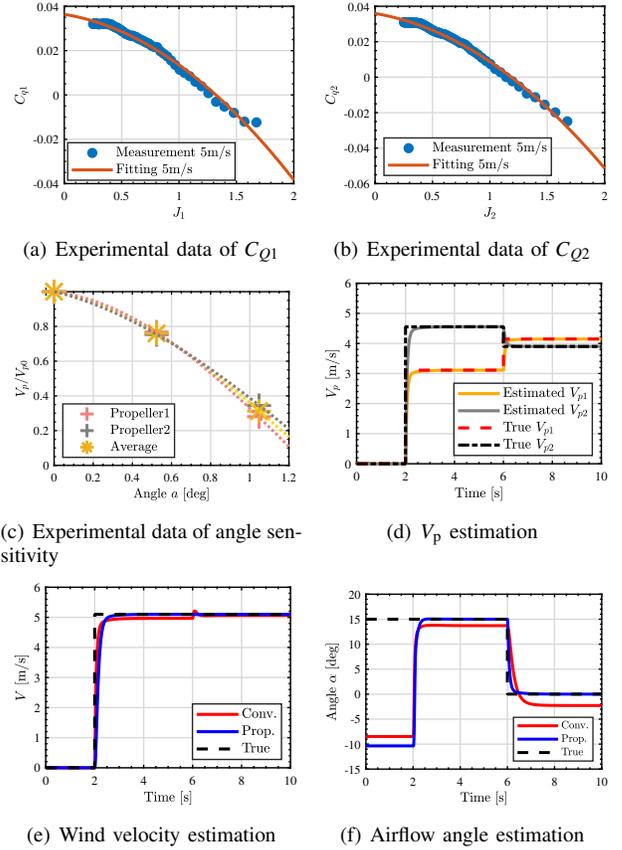
Fig. 5. Propeller characteristics and simulation of wind vector estimation.

IV. SIMULATION

Simulations are conducted to verify the proposed method. Two propellers are used in the simulations to simplify the situations. The wind velocity V is 5.1 m/s and the wind starts to flow at $t = 2$ s. The airflow angle varies 15 deg to 0 deg at $t = 6$ s. The poles of observer for ω and Q of both propellers are 12 rad/s and 105 rad/s, respectively. The function of C_Q and the angular sensitivity function are shown in Figs. 5(a)-5(c). Each value of data samples in Figs. 5(a) and 5(b) is the average of the measurements over a five-second period.

Symbol	Definition	Value
$J_{\omega 1}$	Inertia moment of propeller 1	7.2×10^{-5} kgms^2
$J_{\omega 2}$	Inertia moment of propeller 2	1.0×10^{-4} kgms^2
$B_{\omega 1}$	Viscosity coefficient of propeller 1	6.0×10^{-6} Nms/rad
$B_{\omega 2}$	Viscosity coefficient of propeller 2	1.7×10^{-6} Nms/rad
T_{c1}	Coulomb friction of motor 1	1.5×10^{-3} N m
T_{c2}	Coulomb friction of motor 2	3.8×10^{-3} N m
K	Torque constant	30.2×10^{-3} Nm/A
D_{p}	Propeller diameter	0.2 m
ρ	Air density	1.26 kg/m^3
σ	Angle between two propellers	51.3 deg
w_1	Angle sensitivity parameter 1 of propeller 1	1.12
ψ_1	Angle sensitivity parameter 2 of propeller 1	0.12
w_2	Angle sensitivity parameter 1 of propeller 2	0.89
ψ_2	Angle sensitivity parameter 2 of propeller 2	0.30
w	Angle sensitivity parameter 1 of method 1	1.01
ψ	Angle sensitivity parameter 2 of method 1	0.20
λ	Weighting factor of RLS	0.995
δ	Threshold of RLS	0.5
d	Step size of optimization	0.005

Each value of data samples in Fig. 5(c) is the average of the measurements over a sixteen-second period at 2500 rpm. Both functions of C_Q and angular sensitivity function are measured under the wind velocity of 5 m/s. In addition, each value of C_Q is measured by changing the rotational speed of the propeller n. Other conditions of simulations are shown in Table I.

A. Estimation of Airflow Velocity Flowing in Propellers

Fig. 5(d) shows the results of the V_{p} estimation of each propeller. As shown in Fig. 5(d), it is confirmed that the velocity V_{p} of the airflow into the propeller is successfully estimated. Note that the true value of V_{p} for each propeller is different even at $\alpha = 0$ deg where the airflow symmetrically flows into propeller 1 and propeller 2. This is because of the difference of the angular sensitivity function of each propeller.

B. Estimation of Wind Vector

Figs. 5(e) and 5(f) show the results of the estimation of wind velocity V and airflow angle α. As shown in Figs. 5(e) and 5(f), the estimate of wind velocity V and airflow angle α has steady-state error in the conventional method. On the other hand, the wind vector is estimated without error by using the proposed method. Note that the airflow angle is not defined during the period from $t = 0$ s to $t = 2$ s because no airflow is flowing in. The delay of the estimation of α is adjusted by d of optimization and λ of RLS.

V. EXPERIMENTS OF WIND VECTOR ESTIMATION

A. Experimental Setup

The wind tunnel experiment is conducted to examine the accuracy and the responsiveness of the proposed method. The rotational speed of the propeller is 2500 rpm. The poles of observer for ω and Q are 12 rad/s and 105 rad/s. $\lambda = 0.995$ at 1 ms sampling cycle and $d = 0.001$. Figs. 6–7 show a picture and diagram of the experimental setup. The function of C_Q in Figs. 5(a)–5(b) and the function of the angular
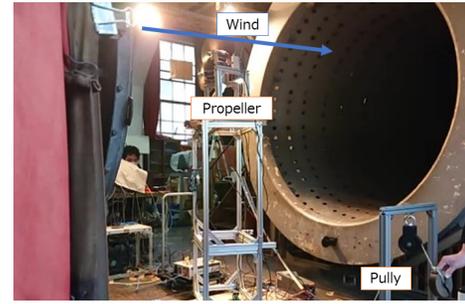
Fig. 6.   Experimental setup of step airflow estimation
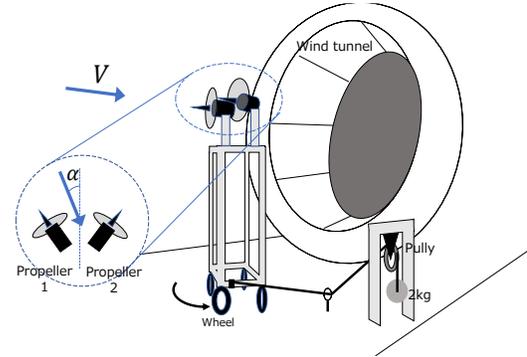
Fig. 7.   Diagram of experimental setup

sensitivity in Fig. 5(c) are also used in the experiment. Step airflow angle is estimated in this experimental setup in this paper. As shown in Fig. 7, the step angle is set 15 deg to 0 deg by using pully and 2 kg weight. The experiment is conducted five times with the same parameters. The value of the pitot tube measured at $t = 0$ s is used as the true value of wind velocity. The true value of airflow angle is obtained by using laser rangefinder LKG-3000 series. APC 9×8E-3 propeller, Maxon DC motor, Maxon 10 bit encoder, and Maxon motor driver ESCON70/10 are used. The other experimental conditions are the same as in Table I.

B. Experimental Results of Wind Vector Estimation

The wind tunnel experiment results of wind vector estimation are shown in Figs. 8 and 9. Solid lines show the average of the five times measurement of each parameter and translucent areas show the standard deviation of the measurement of five times estimation. From Figs. 8 and 9, it is shown that wind vector estimation with step airflow angle is achieved by both the conventional method and the proposed method. The Root Mean Square Error (RMSE) of the average of the five times estimation of wind velocity and airflow angle is shown in Table II. Focusing on the result of Fig. 9(a), the

TABLE II

RMSE OF FIVE TIMES ESTIMATION AVERAGE

	Airflow angle [deg]	Wind velocity [m/s]
Conv.	2.19	0.19
Prop.	0.88	0.11
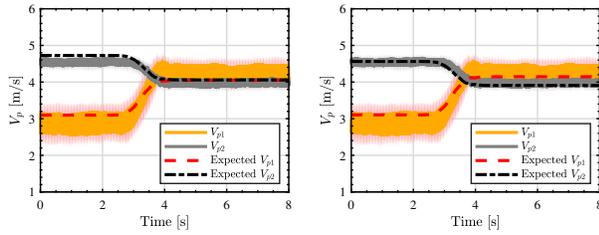
(a) V_p and expected V_p (Conv.)   (b) V_p and expected V_p (Prop.)

Fig. 8.   Result of V_p estimation.
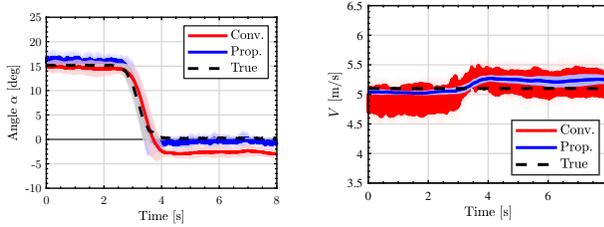
(a) Airflow angle estimation   (b) Wind velocity estimation

Fig. 9.   Result of wind vector estimation.

estimation error of the proposed method is smaller than the conventional method. The reason of the result is considered that the proposed method takes into account the difference of the angular sensitivity function of each propeller. In addition, the conventional method estimates wind velocity by using estimated airflow angle α and estimated V_p directly, which causes estimation noise. On the other hand, according to Fig. 9(b), the wind velocity estimation of proposed method is considered to be less affected by the noise of V_p and α because the proposed method estimates wind velocity and airflow angle simultaneously. However, the estimation error of proposed method would be also larger if the model itself has error. The estimation speed and noise of the wind vector are also adjusted by changing observer poles and λ of RLS and optimization step size d in the experiments. The step size d is chosen so that estimation speed of airflow angle is not slower than estimation speed of RLS in this paper.

VI. Conclusion

In this study, a wind vector estimation method for large industrial fully actuated drones which can improve the accuracy of the conventional method is proposed. The simulations and wind tunnel experiments are conducted to verify the effectiveness of the proposed method. The results of the experiments indicate the superiority of the proposed method in accuracy and noise suppression. Note that the wind vector estimation method in this paper still has difficulty in estimating wind vectors at high rotational speed as the same in [12]. In addition, the experiments only consider static rotational speed and wind speed. Considering these challenges, future work subjects include reconsidering the model of propeller characteristics to improve the accuracy of wind vector estimation at the wide range of rotational speed of the propeller. Moreover, the method in this paper assumes

that airflow flows in only from front side of propellers. Therefore, considering the airflow from the back side of propellers is also a future work.

REFERENCES

[1] K. Nonami, "Research and development of drone and roadmap to evolution," *Journal of Robotics and Mechatronics*, vol. 30, no. 3, pp. 322–336, 2018.

[2] W. Ong, S. Srigrarom, and H. Hesse, "Design methodology for heavy-lift unmanned aerial vehicles with coaxial rotors," in *AIAA Scitech 2019 Forum*, p. 2095, 2019.

[3] A. Poultney, C. Kennedy, G. Clayton, and H. Ashrafiuon, "Robust tracking control of quadrotors based on differential flatness: Simulations and experiments," *IEEE/ASME Transactions on Mechatronics*, vol. 23, no. 3, pp. 1126–1137, 2018.

[4] P.-X. Wu, C.-C. Yang, and T.-H. Cheng, "Cooperative transportation of uavs without inter-uav communication," *IEEE/ASME Transactions on Mechatronics*, 2023.

[5] B. B. Kocer, G. S. G. Lee, and T. Tjahjowidodo, "Nonlinear predictive uav-elastic tool interaction control in real-time," in *2018 IEEE/ASME international conference on advanced intelligent mechatronics (AIM)*, pp. 472–477, IEEE, 2018.

[6] Y. Su, L. Ruan, P. Yu, C.-H. Pi, M. J. Gerber, and T.-C. Tsao, "A fast and efficient attitude control algorithm of a tilt-rotor aerial platform using inputs redundancies," *IEEE Robotics and Automation Letters*, vol. 7, no. 2, pp. 1214–1221, 2021.

[7] T. Magariyama and S. Abiko, "Seamless 90-degree attitude transition flight of a quad tilt-rotor uav under full position control," in *2020 IEEE/ASME International Conference on Advanced Intelligent Mechatronics (AIM)*, pp. 839–844, IEEE, 2020.

[8] R. Rashad, D. Bicego, R. Jiao, S. Sanchez-Escalonilla, and S. Stramigioli, "Towards vision-based impedance control for the contact inspection of unknown generically-shaped surfaces with a fully-actuated uav," in *2020 IEEE/RSJ International Conference on Intelligent Robots and Systems (IROS)*, pp. 1605–1612, IEEE, 2020.

[9] T. Tomić and S. Haddadin, "Simultaneous estimation of aerodynamic and contact forces in flying robots: Applications to metric wind estimation and collision detection," in *2015 IEEE International Conference on Robotics and Automation (ICRA)*, pp. 5290–5296, IEEE, 2015.

[10] P. P. Neumann and M. Bartholmai, "Real-time wind estimation on a micro unmanned aerial vehicle using its inertial measurement unit," *Sensors and Actuators A: Physical*, vol. 235, pp. 300–310, 2015.

[11] T. Tomić, P. Lutz, K. Schmid, A. Mathers, and S. Haddadin, "Simultaneous contact and aerodynamic force estimation (s-cafe) for aerial robots," *The International Journal of Robotics Research*, vol. 39, no. 6, pp. 688–728, 2020.

[12] M. Kamiya, S. Nagai, H. Fujimoto, and K. Suzuki, "Proposal of wind vector estimation using observer for multi-directional propellers drone," in *proceeding of The IEEJ International Workshop on Sensing, Actuation, Motion, Control, and Optimization*, IEEJ, 2023.

[13] K. Takahashi, H. Fujimoto, Y. Hori, H. Kobayashi, and A. Nishizawa, "Modeling of propeller electric airplane and thrust control using advantage of electric motor," in *2014 IEEE 13th International Workshop on Advanced Motion Control (AMC)*, pp. 482–487, IEEE, 2014.

[14] H. Kobayahi, A. Nishizawa, and T. Iijima, "Airspeed estimation by electric propulsion system parameters," in *The 55st Aircraft Symposium*, pp. 869–878, 2017.

[15] K. Yokota and H. Fujimoto, "Pitch angle control by regenerative air brake for electric aircraft," *IEEJ Journal of Industry Applications*, vol. 11, no. 2, pp. 308–316, 2022.

[16] K. Ohnishi, M. Shibata, and T. Murakami, "Motion control for advanced mechatronics," *IEEE/ASME transactions on mechatronics*, vol. 1, no. 1, pp. 56–67, 1996.